



Cite this: *RSC Adv.*, 2024, 14, 38582

# Physicochemical characterization and antibacterial activities of silver nanoparticles prepared by amidated low-methoxyl pectin†

Pei-Jun Li, \*<sup>ab</sup> Run-Sheng Xie,<sup>ab</sup> Jiang-Juan Pan,<sup>b</sup> Yu-Qiu Jiang<sup>ab</sup> and Xing Liu<sup>c</sup>

Pectin-based silver nanoparticles (AgNPs) have been used in the field of antibacterials for food due to their excellent antibacterial properties. Herein, in order to achieve higher antibacterial performance, AgNPs were synthesized using high-methoxyl pectin (HMP) and amidated low-methoxyl pectin (ALMP) as precursors. Initially, ALMP-1, -2, and -4 were obtained by pectin amidation with increasing concentrations of  $\text{NH}_4\text{OH}$ . Later, HMP and ALMPs were used to prepare AgNPs, and their physicochemical property and antibacterial activities were studied. Transmission electron microscopy (TEM) showed that the mean diameters of HMP-Ag and ALMP-4-Ag were  $11.9 \pm 3.8$  and  $13.0 \pm 5.4$  nm, respectively. EDS analysis revealed that ALMP-4-Ag combined with more Ag element than HMP-Ag. X-ray photoelectron spectroscopy (XPS) indicated that ALMP-4-Ag led to a lower ratio of  $\text{Ag}^0$  to  $\text{Ag}^+$  on the surface of AgNPs. Interestingly, ALMP-4-Ag had the strongest antimicrobial effect against *Escherichia coli* and *Staphylococcus aureus*, with the lowest inhibitory concentrations (MICs) of up to  $33 \mu\text{g mL}^{-1}$ , which was 16-fold enhanced compared with HMP-Ag (MICs =  $533 \mu\text{g mL}^{-1}$ ). Finally, ALMP-4-Ag-treated cells revealed higher levels of protein and sugar leakage as well as increased levels of reactive oxygen species (ROS) and malondialdehyde (MDA) than HMP-Ag.

Received 1st October 2024  
Accepted 15th November 2024

DOI: 10.1039/d4ra07060g

rsc.li/rsc-advances

## 1. Introduction

The World Health Organization (WHO) has reported that antibiotic-resistant bacteria kill  $\approx 700\,000$  people every year globally, and this number is predicted to increase to 10 million deaths by 2050 with an estimated economic cost of 100 trillion USD.<sup>1</sup> Among the various antimicrobial products, silver nanoparticles (AgNPs) have been demonstrated to be active in treating several multidrug-resistant bacterial infections.<sup>2,3</sup> In general, AgNPs are synthesized using surfactants, reducing agents, and hazardous chemicals, which have toxic and harmful effects on the environment and human health.<sup>4,5</sup>

In order to solve the above problems and develop alternatives, more environmentally friendly methods are used for synthesizing AgNPs. Renewable plant polysaccharides are highlighted as attractive biopolymers for the synthesis of AgNPs, due to their ability to chelate different metal ions.<sup>6</sup> These polysaccharides can act as both stabilizing agents,

helping to prevent AgNPs from aggregating, and as reducing agents, facilitating the reduction of silver ions to form AgNPs.<sup>7</sup> Pectin is a natural polysaccharide obtained from fruit extracts and mainly consists of chains of D-galacturonic acid units joined by glycosidic linkages, which form the structural backbone of pectin molecules. The alcoholic functions of the galacturonic acid units are efficient  $\text{Ag}^+$  reductants, as has been shown in the synthesis of AgNPs.<sup>8–10</sup>

Pectin-based AgNPs are suitable for various applications, especially in the food industry, due to their low toxicity, excellent antibacterial properties, and favorable mechanical properties. Shankar *et al.*<sup>11</sup> synthesized pectin/AgNPs nanocomposite films, which exhibited strong antibacterial activity against food-borne pathogenic bacteria. Ardjoum *et al.*<sup>12</sup> reported the *in situ* synthesis of AgNPs in a pectin matrix using  $\gamma$ -irradiation and the preparation of antibacterial pectin-based nanocomposite films. Our research group prepared pectin-based AgNPs through a reaction involving silver nitrate and alkali hydrolyzed pectin under microwave irradiation, resulting in the formation of AgNPs with significant antibacterial and antifungal activities.<sup>13</sup> In another study, uniform and stable hesperidin–pectin AgNPs were prepared, and the combination of hesperidin and pectin resulted in a synergistic effect, significantly enhancing the antibacterial properties of AgNPs.<sup>4</sup> Our recent study showed that the synthesis of pectin nanosilver sponges (PE-S/Ag), through an *in situ* freeze-drying process resulted in sponge materials with

<sup>a</sup>Guangdong Provincial Key Laboratory of Utilization and Conservation of Food and Medicinal Resources in Northern Region, College of Food Science & Technology, Shaoguan University, Shaoguan 512005, China

<sup>b</sup>College of Chemistry and Bioengineering, Guilin University of Technology, Guilin 541004, China

<sup>c</sup>Institute for Agro-food Standards and Testing Technology, Shanghai Academy of Agricultural Sciences, Shanghai, 201403, China

† Electronic supplementary information (ESI) available. See DOI: <https://doi.org/10.1039/d4ra07060g>



superior sponge properties, good antibacterial properties, and coagulation properties.<sup>14</sup>

Although pectin-based AgNPs exhibit some level of antibacterial activity, their antibacterial efficiency can be further improved. Currently, pectin is mostly modified in order to obtain some specific properties, including by substitution (alkylation, amidation, quaternization, thiolation, sulfation, oxidation, *etc.*), chain elongation (cross-linking and grafting), and depolymerization (chemical, physical, and enzymatic degradation).<sup>15</sup> However, there have been relatively few reports on the biosynthesis of AgNPs by using modified pectin. In one though, Hileuskaya *et al.*<sup>10</sup> prepared AgNPs by using different types of pectin, including high-methoxyl pectin (HMP-Ag), low-methoxyl pectin (LMP-Ag), and amidated low-methoxyl pectin (ALMP-Ag), and ALMP-Ag displayed the lowest antibacterial activity compared to the others. Interestingly, however, the present work showed different results, with ALMP-Ag exhibiting significantly higher antibacterial activity than HMP-Ag, and the antibacterial activities of ALMP-Ag increased with the acylation degree of pectin. We speculated that the acyl and  $-NH_2$  groups of ALMP played an important role in the reduction of  $Ag^+$ , which led to alterations in the physicochemical properties of the resulting AgNPs and had implications for their antibacterial activities.

On this basis, the main objective of the present study was to investigate how specific characteristics of ALMP, such as the degree of esterification, type of functional groups (including acyl and  $-NH_2$  groups), and molecular weight, influence the properties of the AgNPs, as well as to assess the antibacterial activities of these pectin-based AgNPs. Based on this, we synthesized AgNPs using HMP and ALMP, both of which served as reducers and stabilizers. First, we investigated various properties of the modified pectin, including the galacturonic acid content, degree of esterification, degree of amidation, and molecular weight. Second, the AgNPs were characterized by UV-vis spectroscopy, zeta potential analysis, Fourier transform infrared spectroscopy (FTIR), X-ray diffraction (XRD), XPS, *etc.* Finally, the antibacterial properties of the synthesized AgNPs were evaluated against both Gram-positive and Gram-negative bacteria, and the antibacterial mechanism was revealed through investigating the generation of reactive oxygen species (ROS), the levels of malondialdehyde (MDA), and the leakage of proteins and sugars within bacterial cells.

## 2. Experimental section

### 2.1. Materials

High-methoxyl pectin (HMP, from citrus peel, P9135, galacturonic acid  $\geq 74.0\%$ ) and polygalacturonic acid were supplied by Sigma-Aldrich; silver nitrate ( $AgNO_3$ , AR, purity  $\geq 99.8\%$ ) was purchased from Xilong Scientific Co., Ltd (Shantou, China); the nutrient broths used for the antibacterial activities tests were purchased from Qingdao Hope Bio-Technology Co., Ltd (Qingdao, China); DCFH-DA kit was purchased from Shanghai Qiaoxing Trading Co., Ltd (Shanghai, China); the protein detection kit was purchased from Xian Hete Biotechnology Co., Ltd (Xian, China). All other reagents used in the study were

analytically pure. *E. coli* (strain number: 133264) and *S. aureus* (strain number: 186335) were purchased from Beijing Beina Chuanglian Biotechnology Research Institute (Beijing, China).

### 2.2. Preparation of amidated low-methoxyl pectin (ALMP) and AgNPs

ALMP was prepared following a modified version of the method previously described in the literature.<sup>16</sup> Briefly, a 3.0 g sample of HMP was dissolved in 50 mL of distilled water and stored at 5 °C. At the same time, 40 mL of  $NH_4OH$  (1, 2, and 4 M) and isopropanol mixtures (60%, v/v) were prepared and stored at 5 °C, respectively.  $NH_4OH$  demethylation was started by mixing the samples and solutions in Erlenmeyer flasks and continuously stirring the reaction mixtures at 5 °C for 40 min. These samples were immediately filtered, and rapidly washed with 60% isopropanol, followed by a wash with 1 M HCl in 60% isopropanol. The filter cake was then stirred with acid alcohol for 20 min to remove ammonia present in the salt form. The samples were washed with isopropanol, dried at 60 °C, ground, and analyzed. The ALMPs prepared with different concentrations of  $NH_4OH$  (1, 2, and 4 M) were named as ALMP-1, ALMP-2, and ALMP-4, respectively.

The biosynthesis of the pectin-based AgNPs was conducted with some modifications based on our previous methods.<sup>13</sup> Briefly, 0.2 g of pectin powder was dissolved in 100 mL of NaOH aqueous solution ( $1\text{ g L}^{-1}$ , w/v), and the mixtures were prepared by adding 2 mL of  $0.5\text{ mol L}^{-1} AgNO_3$  (final concentration of  $2\text{ g L}^{-1}$  pectin and  $10\text{ mmol L}^{-1} AgNO_3$ ). The prepared solutions were then exposed to microwave radiation (Galanz, 100 Hz) at 400 W for 2 min. The slurry of AgNPs obtained was washed three times, with distilled water and dried in a hot air oven to obtain the powder. In this study, the AgNPs prepared using high-methoxyl pectin were referred to as HMP-Ag, and the AgNPs prepared using different ALMPs were named as ALMP-1-Ag, ALMP-2-Ag, and ALMP-4-Ag, respectively.

### 2.3. Characterization of HMP, ALMP, and AgNPs

**2.3.1. Galacturonic acid (GA) content, degree of esterification (DE), and degree of amidation (DA).** The GA content was determined according to our previous method<sup>17</sup> and the DE and DA values were determined according to previous methods in the literature.<sup>18</sup> Briefly, a sample of HMP/ALMP (100 mg) was dissolved in 100 mL carbon dioxide-free water. Next, 5 drops of phenolphthalein reagent were added, and the sample was titrated with 0.1 M NaOH ( $V_1$ , in mL). Then, 20 mL of 0.5 M NaOH was added, and the mixture was allowed to stand for 15 min. Next, 20 mL of 0.5 M HCl was added, and the solution was shaken vigorously until the pink color disappeared. Five drops of phenolphthalein were added again, and the solution was titrated with 0.1 M NaOH until a pale pink color was obtained ( $V_2$ , in mL).

The solution was transferred to a distillation flask, and an extension tube of the condenser was inserted into a receiving bottle containing 150 mL of carbon dioxide-free water and 20 mL of 0.1 M HCl. Next, 20 mL of 0.5 M NaOH solution was added, and the solution was heated and distilled until 80–120 mL of distillate was collected. Then methyl red indicator was added,



and the solution was titrated with a 0.1 M NaOH standard solution until the red color disappeared (S, mL). Another 20 mL of 0.1 M HCl solution used as a blank test (B, mL) was titrated with the 0.1 M NaOH standard solution. The amido titration was calculated as (B–S) and recorded as “V<sub>3</sub>”. The formulas for calculating the DE and DA contents were as follows:

$$DE(\%) = \frac{V_2}{V_1 + V_2 + V_3} \times 100 \quad (1)$$

$$DA(\%) = \frac{V_3}{V_1 + V_2 + V_3} \times 100 \quad (2)$$

**2.3.2. High-performance size-exclusion chromatography (HPSEC).** The molecular weight distributions of the target products were assessed using HPSEC.<sup>19</sup> The instrument consisted of an Agilent 1100 chromatographic instrument and a Shodex OHPak SB-804HQ (8 mm ID × 300 mm L), operating at 35 °C with a RID-10A detector (SHIMADZU). The mobile phase was a phosphate buffer consisting of 0.0177 M NaH<sub>2</sub>PO<sub>3</sub> and 0.0079 M Na<sub>2</sub>HPO<sub>3</sub>, with a flow rate of 0.5 mL min<sup>−1</sup>. Shodex Standard P-82 Pullulan (*M<sub>w</sub>* 6.2, 10.0, 21.7, 48.8, 113, and 210 kDa) was used as the calibration standard.

**2.3.3. Characterization of AgNPs.** According to previous methods,<sup>20</sup> the AgNPs in colloidal solution were monitored using a UV-vis spectrophotometer (TU-1950, Beijing, China), zeta sizer Nano ZS90 (Malvern Instruments, Malvern, UK), and transmission electron microscopy system (TEM, JEOL-JEM-2100F, Japan), respectively. The dried AgNPs powders were subjected to FE-SEM (S-5000, Hitachi Co., Ltd, Matsuda, Japan), X-ray diffraction (XRD, PANalytical B. V., X'Pert3 Powder), thermogravimetric analysis (SDT Q600, TA Instruments), and FTIR spectroscopy (Nicolet 10, Thermo Fisher Scientific, Waltham, MA, USA), respectively. Also, X-ray photoelectron spectroscopy (XPS, ESCALAB 250Xi, Thermo Fisher Scientific, USA) was conducted to determine the chemical states and composition of the surface of the AgNPs.

## 2.4. Antibacterial activities

The minimum inhibitory concentration (MIC) was determined as the lowest concentration of the test compound that inhibited the visible growth of bacteria, as confirmed by measuring the OD<sub>600</sub> for all the samples.<sup>16</sup> Here, 3.2 mg AgNPs powder was ultrasonically dispersed in LB broth (1 mL), and gradient dilution was performed to obtain AgNPs suspensions at concentrations of 0, 0.2, 0.4, 0.8, 1.6, and 3.2 mg mL<sup>−1</sup>. In the experiment, the LB broth (200 μL), AgNPs suspension (50 μL), and bacterial suspension (50 μL) were thoroughly mixed and placed into well plates, with AgNPs concentrations of 0, 33, 67, 133, 267, and 533 μg mL<sup>−1</sup> in each well, respectively. The cultures were incubated at 37 °C for 24 h, and the absorbance of the cultures at 600 nm was measured every 3 h using a microplate reader.

## 2.5. Antibacterial mechanism

**2.5.1. Intracellular components leakage.** The leakage of intracellular compounds reflects the permeability of the

bacterial cell membrane and cell wall.<sup>21</sup> Briefly, AgNPs dilutions (3 mL, 3.2 mg mL<sup>−1</sup>) were added to *E. coli* suspension (15 mL, 1 × 10<sup>5</sup> CFU mL<sup>−1</sup>), and cultured at 37 °C for 0 and 24 h, respectively. A BCA protein assay kit (Xian Hat Biotechnology Co., Ltd, China) was used to determine the extracellular protein concentration of the bacteria suspension. The content of released reducing sugar in the treated broth was determined using the DNS method.<sup>22</sup>

**2.5.2. Intracellular ROS level evaluation.** A fluorescence spectrometer was used to measure the intracellular ROS level in response to AgNPs stress. The excitation wavelength was fixed at 488 nm and the emission wavelength was scanned at 525 nm. AgNPs dilutions (3 mL, 3.2 mg mL<sup>−1</sup>) were added to the bacteria suspension (15 mL, 1 × 10<sup>6</sup> CFU mL<sup>−1</sup>), cultured at 37 °C for 0 and 6 h, and then centrifuged at 4 °C and 2400 rpm for 15 min. After centrifugation, 2 mL of the supernatant was collected and added into a sealed culture tube, and 3 mL of a diluted DCFH-DA reagent (Qiaoxingmaoyi Co., Ltd, Shanghai, China) was added. After full mixing, the bacteria were cultured at 37 °C for 1 h, and centrifuged at 2400 rpm at 4 °C for 10 min. The supernatant was used to determine the fluorescence intensity at 0 and 6 h, respectively.

**2.5.3. MDA measurements.** MDA levels were measured according to the previous method.<sup>23</sup> Briefly, *E. coli* were cultured at 37 °C for 48 h in 150 mL of LB medium, and the samples were collected at 0 and 6 h after exposure to AgNPs treatment (533 μg mL<sup>−1</sup>, w/v), respectively. The culture medium was collected and centrifuged at 8000 rpm for 10 min, and the *E. coli* cells were obtained. The bacterial cells were disrupted using liquid nitrogen grinding and mixed with 3 mL of trichloroacetic acid (5%, v/v) and 3 mL of freshly prepared thiobarbituric acid (TBA) (0.5%, w/v). The mixture was incubated at 110 °C for 30 min. The reaction was allowed to cool to room temperature and then centrifuged at 5000 rpm for 10 min. The OD of the supernatant was measured at 450, 532, and 600 nm, respectively. The MDA level was calculated using the following formula.

$$MDA [mmol g^{-1}] = [6.452 \times (A_{532} - A_{600}) - 0.559 \times A_{600}] \times V_t / (V_s \times W) \quad (3)$$

where *V<sub>t</sub>* is the total volume of the extract, *V<sub>s</sub>* is the testing volume of the extract, and *W* is the weight of *E. coli* cells.

# 3. Results and discussion

## 3.1. Preparation and physicochemical properties of ALMP

In this work, ALMP-1, ALMP-2, and ALMP-4 were obtained by subjecting pectin to amidation with increasing concentrations of NH<sub>4</sub>OH. As shown in Table 1, with the increase in ammonia concentration, the GA content in pectin increased from 70.5% ± 1.4% to 89.1% ± 0.8%, suggesting that the alkaline hydrolysis process led to the reduction of heteropolysaccharides in the pectin hair zone. Meanwhile, the DE value of amidated pectin decreased significantly with the higher ammonia concentrations, which was consistent with previous research.<sup>24</sup> After 40 min, the DE value of pectin decreased from an initial value of 85.7% ± 0.8% to 38.6% ± 0.9%, and higher concentrations of



Table 1 Qualitative and quantitative characteristics of HMP, ALMP-1, ALMP-2, and ALMP-4<sup>a</sup>

| Materials | Properties |             |             |             |                            |
|-----------|------------|-------------|-------------|-------------|----------------------------|
|           | PY (%)     | GA (%)      | DE (%)      | DA (%)      | <i>M<sub>w</sub></i> (kDa) |
| HMP       | —          | 70.5 ± 1.4a | 85.7 ± 0.8a | 0.0 ± 0.1a  | 308.5 ± 9.2a               |
| ALMP-1    | 87.8 ± 0.8 | 78.4 ± 2.8b | 66.2 ± 1.1b | 3.2 ± 0.1b  | 261.5 ± 5.9b               |
| ALMP-2    | 86.8 ± 1.0 | 81.8 ± 2.2b | 45.7 ± 0.5c | 9.6 ± 0.6c  | 215.1 ± 4.7c               |
| ALMP-4    | 86.7 ± 1.3 | 89.1 ± 0.8c | 38.6 ± 0.9d | 18.6 ± 0.9d | 196.5 ± 6.1d               |

<sup>a</sup> Note: PY – pectin yield, GA – galacturonic acid, DE – degree of esterification, DA – degree of amidation. Means within different letters (a, b, c, and d) are significantly different ( $p < 0.05$ );  $n = 3$ .

ammonia led to lower DE values. In addition, the degrees of amidation (DA) of ALMP-1, ALMP-2, and ALMP-4 were  $3.2\% \pm 0.1\%$ ,  $9.6\% \pm 0.6\%$ , and  $18.6\% \pm 0.9\%$ , respectively (Table 1). This data indicated that more amide groups were formed by treatment with higher concentrations of  $\text{NH}_4\text{OH}$ .

Molecular weight is an important indicator of the physical, chemical, and structural properties of polysaccharides. The size and distribution of the molecular weight directly affect the digestion, absorption, and biological activity of polysaccharides.<sup>19</sup> The molecular weight distributions of pectin and amidated pectin are shown in Fig. S1.† Table 1 also shows that the  $M_w$  values of HMP, ALMP-1, ALMP-2, and ALMP-4 were  $308.5 \pm 9.2$ ,  $261.5 \pm 5.9$ ,  $215.1 \pm 4.7$ , and  $196.5 \pm 6.1$  kDa, respectively. This suggests that  $\beta$ -degradation resulted in the chain breakage of the pectin chain with the amidated modification, which led to a decrease in the molecular weight of pectin. These findings illustrate that the concentration of ammonia during the amidation process affected the chemical composition and molecular characteristics of the modified pectin samples. In a previous report, the extent of ammonolysis and hydrolysis of pectin in aqueous solution were reported to be highly dependent on ammonia concentration and temperature.<sup>24</sup>

### 3.2. Characterization of AgNPs

**3.2.1. UV-vis spectrum, zeta potential, and particle size distribution.** In general, different metal nanoparticles exhibit distinct positions of absorption peaks in the UV-vis spectrum, and AgNPs show a strong and characteristic absorption peak at around 410 nm.<sup>4</sup> The presence of a symmetric band in the absorption spectra with a maximum at 403–410 nm is indicative of the presence of AgNPs in the solution (Fig. 1a and Table 2). It is well known that the wavelength of the surface plasmon resonance (SPR) band maximum is correlated with the size of  $\text{Ag}^0$  nanoparticles, and its full width at half maximum (FWHM) determines the size distribution (dispersity) of the nanoparticles.<sup>10</sup> Among the synthesized samples, ALMP-Ag turned out to be the most monodispersed with a FWHM of less than 100 nm, while the most polydispersed sample was formed in the presence of HMP-Ag (Table 2).

Fig. S2 and S3† show the hydrodynamic diameters and zeta potential values of the AgNPs, respectively. According to Table 2, the  $d_H$  values (hydrodynamic diameter of NPs measured with DLS) of ALMP-Ag were lower than those of HMP-Ag, and ALMP-

4-Ag showed the minimum particle size value. Contrary to this finding, Hileuskaya *et al.*<sup>10</sup> reported that the mean diameter of HMP-Ag was lower than that of ALMP-Ag. This inconsistency could be attributed to the different synthesis process and physicochemical properties of ALMP-Ag. In addition, HMP-Ag showed more negative surface charges than ALMP-Ag, which indicated that the acylation reaction reduced the negative charges of pectin macromolecules.

**3.2.2. FTIR, XRD, XPS, and TGA analyses.** The functional groups of pectin and AgNPs were detected by FTIR to aid analyzing the synthesis mechanism of the AgNPs (Fig. 1b). The bands at  $3448\text{ cm}^{-1}$  (O–H),  $2941\text{ cm}^{-1}$  (C–H),  $1745\text{ cm}^{-1}$  (C=O of nonionic carboxy groups),  $1637\text{ cm}^{-1}$  (–C=O), and  $1088\text{ cm}^{-1}$  (C–OH) were various characteristic bands of free pectin.<sup>20</sup> In the IR spectrum of the ALMP-4 sample, the band at

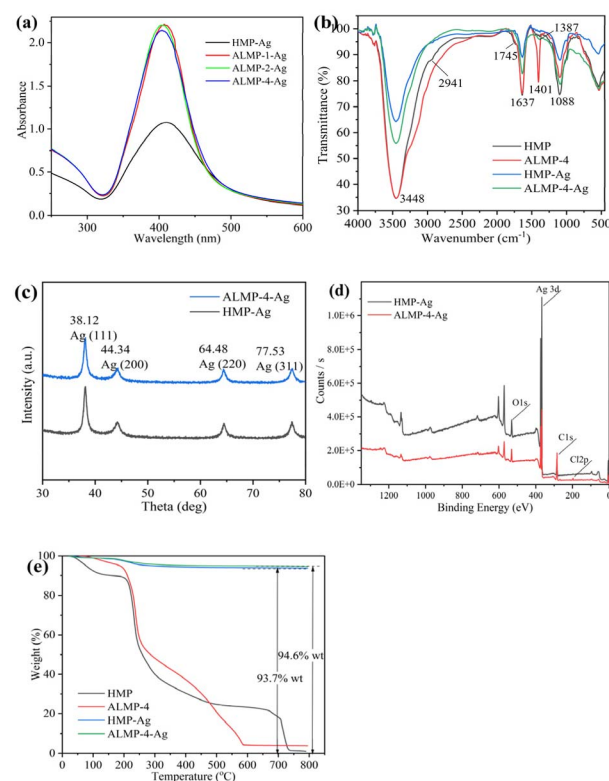


Fig. 1 UV-vis absorption spectroscopy (a), FTIR spectroscopy (b), XRD (c), XPS full spectrum (d), and TGA (e) analyses of HMP and ALMP-Ag.





Table 2 Characteristics and antibacterial activities of AgNPs<sup>a</sup>

| AgNPs     | Characteristics of AgNPs    |          |                       |                       |                         | MIC values ( $\mu\text{g mL}^{-1}$ ) |                  |
|-----------|-----------------------------|----------|-----------------------|-----------------------|-------------------------|--------------------------------------|------------------|
|           | $\lambda_{\text{max}}$ , nm | FWHM, nm | $d_{\text{H}}$ , nm   | $d_{\text{TEM}}$ , nm | $\zeta$ -Potential, mV  | <i>E. coli</i>                       | <i>S. aureus</i> |
| HMP-Ag    | 410                         | 111      | $202.4 \pm 2\text{a}$ | $11.9 \pm 3.8$        | $-20.4 \pm 0.3\text{a}$ | 533                                  | 533              |
| ALMP-1-Ag | 407                         | 83       | $174.1 \pm 3\text{b}$ | $12.1 \pm 2.3$        | $-19.2 \pm 1.6\text{a}$ | 267                                  | 267              |
| ALMP-2-Ag | 403                         | 83       | $157.2 \pm 1\text{c}$ | $13.5 \pm 0.7$        | $-16.1 \pm 1.8\text{b}$ | 133                                  | 133              |
| ALMP-4-Ag | 404                         | 85       | $119.1 \pm 2\text{d}$ | $13.0 \pm 5.4$        | $-14.8 \pm 0.8\text{b}$ | 33                                   | 33               |

<sup>a</sup>  $d_{\text{H}}$  – hydrodynamic diameter of NPs measured with DLS,  $d_{\text{TEM}}$  – diameter of NPs measured with TEM, MIC – minimum inhibitory concentration, mean within different letters (a, b, c, and d) are significantly different ( $p < 0.05$ );  $n = 3$ .

$2941\text{ cm}^{-1}$  had disappeared, and a new band at  $1401\text{ cm}^{-1}$  was observed. The results imply that the amidation reaction reduced the –OH group in HMP, and a new amide bond was generated. For the HMP-Ag and ALMP-4-Ag samples, the vibrational band located at  $3448\text{ cm}^{-1}$  was weakened, indicating that O–H exhibited reducing properties and participated in the synthesis process of the AgNPs. The disappearance of the band located at  $1745\text{ cm}^{-1}$  indicated that all the ester groups ( $-\text{COOCH}_3$ ) of HMP and ALMP were hydrolyzed to form  $-\text{COOH}$  under alkaline conditions. After the reduction reaction with  $\text{Ag}^+$ , the IR spectrum of ALMP-4 showed a significant decrease in the amide bond, with the peak shifted from  $1401$  to  $1387\text{ cm}^{-1}$ , indicating that the amide bond was involved in the reduction reaction of  $\text{Ag}^+$ . In conclusion, alkaline conditions caused the  $-\text{COOCH}_3$  of ALMP to be hydrolyzed to form  $-\text{COOH}$ , which combined with  $\text{Ag}^+$  to form a carboxylate.  $\text{Ag}^+$  was then reduced by amide bonding and O–H, resulting in the synthesis of ALMP-Ag.

As shown in Fig. 1c–e, HMP-Ag and ALMP-4-Ag were characterized by XRD, XPS, and TGA, respectively. Fig. 1c shows that XRD peaks could be observed at  $38.12^\circ$ ,  $44.34^\circ$ ,  $64.48^\circ$ , and  $77.53^\circ$ , which were consistent with metallic silver, and in line with previous reports.<sup>25</sup> The complete XPS spectra showed the presence of the elements C, Ag, and O in both HMP-Ag and ALMP-4-Ag (Fig. 1d). Li *et al.*<sup>25</sup> believed that the C and O elements of AgNPs came from precursor pectin macromolecules. The appearance of the Cl element in ALMP-4-Ag was noteworthy, and could be explained by the use of HCl during the amidation reaction. The combustion residues from HMP-Ag and ALMP-4-Ag were 93.7% and 94.6% (w/w), respectively (Fig. 1e), indicating that ALMP-4 combined more Ag than HMP during the synthesis process of the AgNPs.

To identify the metallic components and their reduction degree, XPS spectra were recorded and compared. Deconvolution of the high-resolution XPS spectrum of the Ag 3d revealed the chemical character of Ag in the synthesized AgNPs (Fig. 2). According to the standard spectrum in NIST, the binding energy of  $\text{Ag}^+$  is higher than that of  $\text{Ag}^0$ .<sup>26</sup> In the XPS spectra (Fig. 2b–d), the higher degree of amidation of pectin, the lower the ratio of  $\text{Ag}^0$  to  $\text{Ag}^+$  on the surface of the synthesized ALMP-Ag. This suggests that the surface of AgNPs prepared with higher amidated pectin is more prone to oxidation, forming  $\text{Ag}_2\text{O}$ , and subsequently  $\text{Ag}^+$  is formed in acidic environments. This higher  $\text{Ag}^+$  content likely contributed to their enhanced antibacterial

properties. Zheng *et al.*<sup>27</sup> believed that the generation and release of  $\text{Ag}^+$  ions were often initiated with the oxidation of  $\text{Ag}^0$ , which could trigger the production of ROS and lead to bacterial cell damage, ultimately resulting in an antibacterial effect.

**3.2.3. TEM and SEM images.** In general, DLS and TEM are indispensable technical means used for analyzing the particle size and morphology of nanoparticles. DLS analysis can reveal the hydrodynamic diameter and provides information about the size distribution of NPs with a hydrated polymer shell,<sup>28</sup> while TEM provides high-resolution images of NPs, enabling accurate measurement of the size, shape, and morphology of NPs.<sup>29</sup> Table 2 shows that the average sizes of the AgNPs measured by DLS fell within the range of 25–60 nm. Among the various AgNPs, ALMP-4-Ag had the smallest hydrodynamic diameter, which indicates that ALMP-4-Ag was more monodisperse and had a smaller overall size. However, TEM measurements revealed that the mean diameters of HMP-Ag and ALMP-4-Ag were similar, with values of  $11.9 \pm 3.8\text{ nm}$  and  $13.0 \pm 5.4\text{ nm}$ , respectively (Fig. 3). It can be seen that the TEM particle size of AgNPs obtained in this study was much lower than that of previous studies. Wang *et al.*<sup>30</sup> reported that pectin-stabilized AgNPs exhibited a spherical shape with a mean diameter ranging from 15–20 nm, while Al-Muhanna *et al.*<sup>31</sup> reported the average diameter of NPs synthesized in the presence of ALMP was  $22 \pm 6\text{ nm}$ . It should be noted that

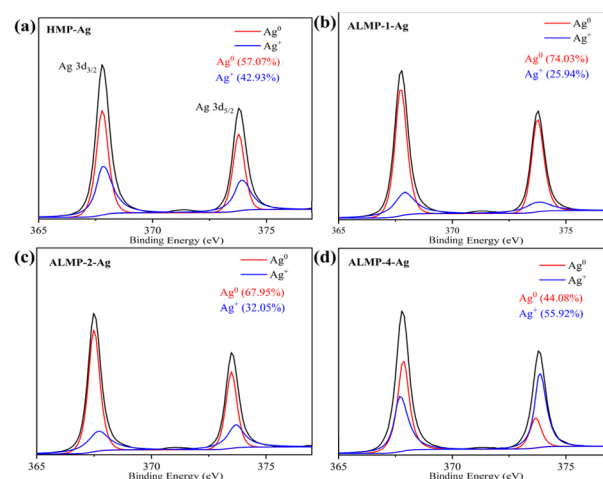


Fig. 2 High-resolution Ag 3d XPS spectra of HMP-Ag (a), ALMP-1-Ag (b), ALMP-2-Ag (c), and ALMP-4-Ag (d).



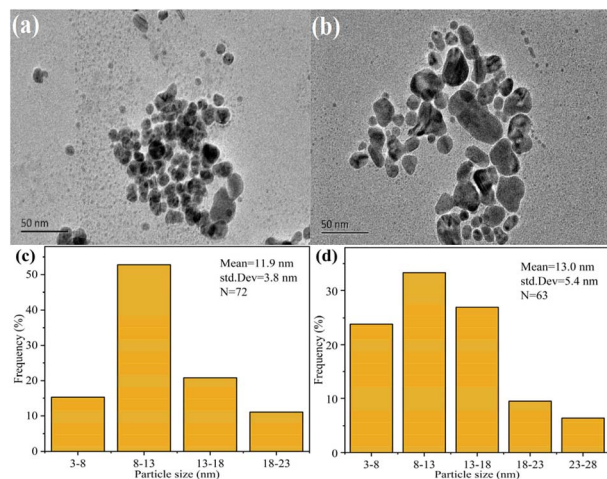


Fig. 3 TEM images and the size distribution of HMP-Ag (a, c) and ALMP-4-Ag (b, d).

the results of the particle-size detection by DLS and TEM were inconsistent for the same nanoparticles. This phenomenon can be explained by the fact that although the sizes of AgNPs' core were similar, the surface coatings on the AgNPs were different, which led to the differences in their hydrodynamic diameters.<sup>32</sup>

Fig. 4a and b show that both AgNPs prepared by HMP and ALMP-4-Ag were uniform spherical particles, while the particle size of the former was smaller than that of the latter. EDS analysis revealed that the main component of both HMP-Ag and ALMP-4-Ag was metallic silver, and the normalized percentages of silver in HMP-Ag and ALMP-4-Ag were 92.08% and 94.18%, respectively (Fig. 4c and d). The results for EDS analysis of the silver elements were highly consistent with the TGA analysis data (Fig. 1e), while the C and O elements were derived from the precursor pectin.

### 3.3. Antibacterial activities of the AgNPs

The antibacterial activities of AgNPs determined by the MIC tests are shown in Table 2 and Fig. 5. After 24 h of incubation,

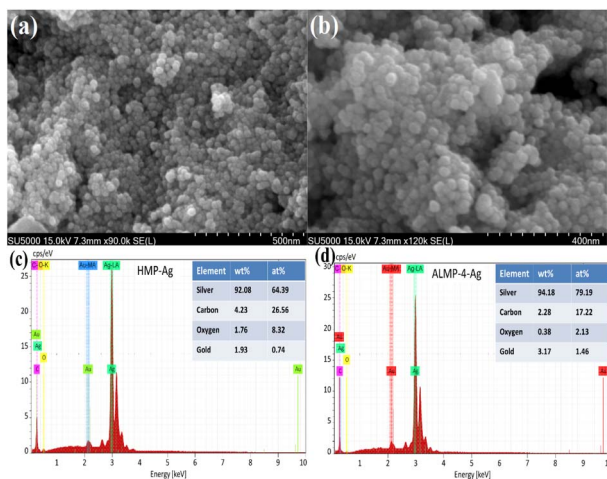


Fig. 4 SEM images and EDS of HMP-Ag (a, c) and ALMP-4-Ag (b, d).

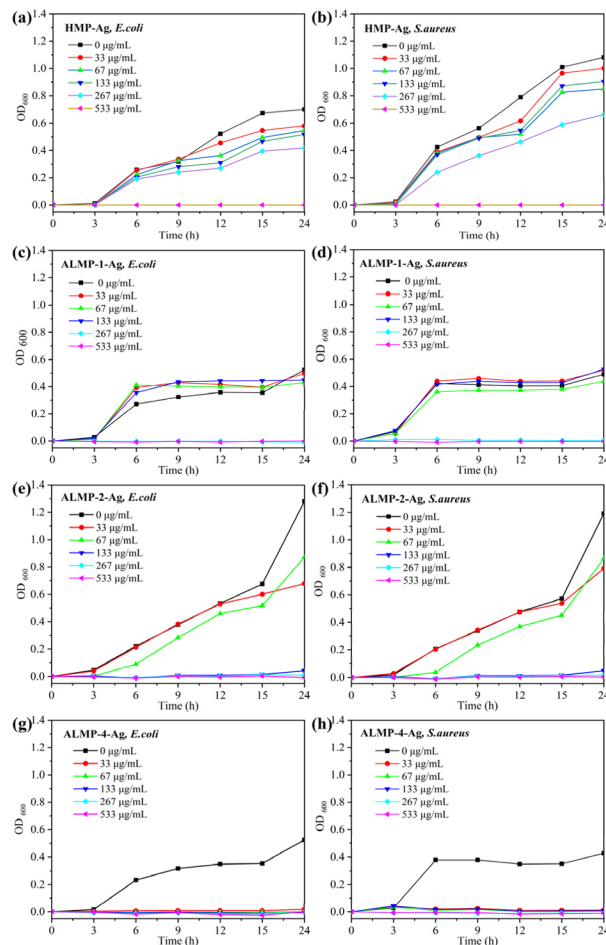


Fig. 5 *E. coli* and *S. aureus* growth curves at HMP-Ag (a, b), ALMP-1-Ag (c, d), ALMP-2-Ag (e, f), and ALMP-4-Ag (g, h), respectively.

the MIC values for HMP-Ag, ALMP-1-Ag, ALMP-2-Ag, and ALMP-4-Ag against both *E. coli* and *S. aureus* were found to be 533, 267, 133, and 33 μg mL<sup>-1</sup>, respectively. ALMP-4-Ag showed an impressive 16-fold increase in bacterial inhibition against *E. coli* and *S. aureus* compared to HMP-Ag. The pectin-based AgNPs previously prepared under microwave irradiation by our research group showed MIC values of 160 mg mL<sup>-1</sup> against *E. coli* and *S. aureus*. Similarly, Ibraheem *et al.*<sup>33</sup> synthesized AgNPs employing *Parkia biglobosa* pectin, demonstrating antibacterial activity at a concentration of 100 μg mL<sup>-1</sup>. Furthermore, Wang *et al.*<sup>34</sup> reported the synthesis of AgNPs from the polysaccharides of walnut green husk, which showed inhibitory effects on *E. coli* and *S. aureus* at a concentration of 50 μg mL<sup>-1</sup>. In this work, the results indicated that the antimicrobial activity of ALMP-4-Ag was superior to that reported in previous studies.

Obviously, the antibacterial activities of ALMP-Ag tended to increase with an increasing DA value and decreasing  $M_w$  of pectin. The results could be explained by the following factors. First, the special structural characteristics of ALMP are one of the important factors, with a higher content of GA, lower DE values, higher DA, and lower  $M_w$  (Table 1), which are different from those of HMP. The higher GA content and lower DE in

ALMP resulted in the presence of more diol moieties in the galacturonic acid units, while the higher DA indicated the presence of more amide groups, and the lower  $M_w$  might provide better accessibility to the functional groups, which is particularly conducive to reducing  $Ag^+$  and facilitating the formation of AgNPs with superior antibacterial properties.<sup>8</sup> However, in a previous report, compared with PectLM-Ag and PectHM-Ag, ALMP-Ag displayed lower antibacterial activities against strains of *Bacillus* bacteria compared to PectLM-Ag and PectHM-Ag, and it displayed no growth suppression against *E. coli*.<sup>10</sup> Although the structural characteristics of ALMP in this work were very similar to those reported in the study of Hileuskaya *et al.* (DE = 32%, DA = 18%,  $M_w$  = 120 kDa), there were still significant differences in the synthesis process of AgNPs, which led to the difference in antibacterial efficiency. Second, the physicochemical properties of AgNPs are another inevitable factor, including the particle size distribution, zeta potential, and the proportion and valence state of Ag elements. Last but not least, the amount of released  $Ag^+$  is also an important factor affecting the antibacterial efficiency of AgNPs.<sup>32</sup> A profound investigation is currently in progress and the obtained data are to be published in the near future. In short, ALMP-4-Ag displayed the highest antibacterial activity against both Gram-positive bacteria and Gram-negative bacteria, with lower MICs compared to previous reports.<sup>10,13</sup>

### 3.4. Antibacterial mechanism of the AgNPs

The disruption of bacterial cell membranes and the subsequent leakage of intracellular components, such as proteins and sugars, is a well-documented antibacterial mechanism of AgNPs.<sup>35</sup> We determined the leakages of intracellular protein and reducing sugar by treating *E. coli* cells with AgNPs at their MIC value of  $533 \mu\text{g mL}^{-1}$ . As shown in Fig. 6a, only a small amount of protein leaked incrementally from the *E. coli* after treatment with HMP-Ag and ALMP-4-Ag for 24 h. Nevertheless, the leakage of

reducing sugar reached 66.9 and  $72.3 \mu\text{g mL}^{-1}$  after treatment with HMP-Ag and ALMP-4-Ag for 24 h, respectively, which were much higher than the control sample (Fig. 6b). All of these results are consistent with previous studies.<sup>35,36</sup>

Generally, ROS are regarded as a collective marker of the superoxide anion, hydroxyl radical, and hydrogen peroxide, which acts as an indicator of oxidative stress.<sup>37</sup> Oxidative stress plays an important role in mediating toxicity in bacterial cells, which can damage bacterial DNA, the cell membrane, and cellular proteins, leading to cell death.<sup>4</sup> Fig. 6c shows that the fluorescence intensity of ROS in each group was basically the same at 0 h, but ROS increased significantly after 6 h of treatment by AgNPs. It is worth noting that the HMP-Ag- and ALMP-4-Ag-treated cells produced increases of ROS of up to 36.9% and 70.0%, respectively, but the untreated treated cells increased by only 7.5%.

Furthermore, oxidative stress can lead to the peroxidation of polyunsaturated lipids, resulting in the production of peroxy radicals and single oxygen.<sup>35,38</sup> MDA is a well-known product of lipid peroxidation and is often used as an important biomarker to assess the extent of oxidative damage to lipids within cells. As shown in Fig. 6d, the levels of MDA in AgNPs-treated cells were significantly higher compared to the untreated cells. The MDA levels were 2.3- and 1.7-folds higher in HMP-Ag- and ALMP-4-Ag-treated *E. coli*, respectively. These findings highlight the antibacterial potential of AgNPs, especially ALMP-4-Ag, as effective antibacterial agents that disrupt bacterial cells through oxidative stress and lipid peroxidation mechanisms.

## 4. Conclusions

Pectin-based AgNPs were synthesized using HMP and ALMP as both reducers and stabilizers. Compared to HMP, the ALMPs exhibited distinctive features, including higher GA content, lower DE values, higher DA, and lower  $M_w$ . Furthermore, ALMP-Ag demonstrated several advantages over HMP-Ag, such as having less negative surface charges, smaller particle size, higher silver content, and lower ratio of  $Ag^0$  to  $Ag^+$  on the nanoparticle surface. Importantly, the antibacterial activity of ALMP-Ag exhibited a positive correlation with the DA of pectin and was inversely correlated with the  $M_w$  of pectin. Among all the tested AgNPs, ALMP-4-Ag had the strongest antibacterial effect against both *E. coli* and *S. aureus* (MIC  $33 \mu\text{g mL}^{-1}$ ), which were much lower than HMP-Ag (MIC  $533 \mu\text{g mL}^{-1}$ ). In brief, the experimental data provided valuable insights into the enhanced antibacterial efficiency of modified pectin-based AgNPs. These findings have significant implications for potential applications in the food and medical industries, where the demand for effective and safe antibacterial agents is high.

## Data availability

Data will be made available on request.

## Author contributions

P. J. L. and R. S. X. conceived the concept and experiments. R. S. X. and J. J. P. carried out the materials synthesis,

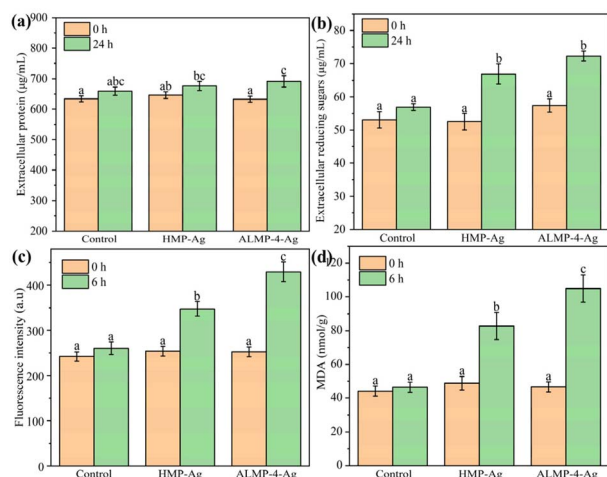


Fig. 6 Production of extracellular protein (a), extracellular reducing sugars (b), intracellular ROS (c), and MDA content (d) in *E. coli* cell suspensions treated with HMP-Ag and ALMP-4-Ag. Means within different letters (a, b, and c) are significantly different ( $p < 0.05$ ;  $n = 3$ ).





characterizations, data curation, writing-original draft, writing-review & editing. P. J. L. carried out the writing-review & editing, supervision, project administration and funding acquisition. Y. Q. J. and X. L. co-wrote the paper and revised the paper. All authors discussed the results and commented on the manuscript.

## Conflicts of interest

There are no conflicts to declare.

## Acknowledgements

This study was financially supported by the Guangxi Natural Science Foundation (2020GXNSFAA297198), the Shaoguan Government-supported Project for Scientific Researchers in 2023 (230324098034896), the Talent Introduction (Training) Project of Shaoguan University (142-9900064701), and the Open Fund of the Guangdong Provincial Key Laboratory of Utilization and Conservation of Food and Medicinal Resources in Northern Region (FMR2022004M).

## References

- 1 Y. Wang, Y. Yang, Y. Shi, H. Song and C. Yu, *Adv. Mater.*, 2020, **32**, 1904106.
- 2 J. M. V. Makabenta, A. Nabawy, C.-H. Li, S. Schmidt-Malan, R. Patel and V. M. Rotello, *Nat. Rev. Microbiol.*, 2021, **19**, 23–36.
- 3 A. Roy, O. Bulut, S. Some, A. K. Mandal and M. D. Yilmaz, *RSC Adv.*, 2019, **9**, 2673–2702.
- 4 Z.-Y. Zhao, P.-J. Li, R.-S. Xie, X.-Y. Cao, D.-L. Su and Y. Shan, *Int. J. Biol. Macromol.*, 2022, **214**, 220–229.
- 5 L. Xu, Y.-Y. Wang, J. Huang, C.-Y. Chen, Z.-X. Wang and H. Xie, *Theranostics*, 2020, **10**, 8996–9031.
- 6 J. R. Nakkala, R. Mata and S. R. Sadras, *J. Colloid Interface Sci.*, 2017, **499**, 33–45.
- 7 H. E. Emam and H. B. Ahmed, *Carbohydr. Polym.*, 2016, **135**, 300–307.
- 8 P. Pallavicini, C. R. Arciola, F. Bertoglio, S. Curtosi, G. Dacarro, A. D'Agostino, F. Ferrari, D. Merli, C. Milanese, S. Rossi, A. Taglietti, M. Tenci and L. Visai, *J. Colloid Interface Sci.*, 2017, **498**, 271–281.
- 9 K. Devasvaran and V. Lim, *Pharm. Biol.*, 2021, **59**, 494–503.
- 10 K. Hileuskaya, A. Ladutska, V. Kulikouskaya, A. Kraskouski, G. Novik, I. Kozerozhets, A. Kozlovskiy and V. Agabekov, *Colloids Surf., A*, 2020, **585**, 124141.
- 11 S. Shankar, N. Tanomrod, S. Rawdkuen and J.-W. Rhim, *Int. J. Biol. Macromol.*, 2016, **92**, 842–849.
- 12 N. Ardjoum, S. Shankar, N. Chibani, S. Salmieri and M. Lacroix, *Food Hydrocolloids*, 2021, **121**, 107000.
- 13 D.-L. Su, P.-J. Li, M. Ning, G.-Y. Li and Y. Shan, *Mater. Lett.*, 2019, **244**, 35–38.
- 14 Z.-Y. Zhao, P.-J. Li, X.-Y. Cao, R.-S. Xie and H.-Y. Li, *Cellulose*, 2023, **30**, 9425–9437.
- 15 J. Chen, W. Liu, C. M. Liu, T. Li, R. H. Liang and S. J. Luo, *Crit. Rev. Food Sci. Nutr.*, 2015, **55**, 1684–1698.
- 16 S. A. Elnawawi and Y. A. Heikal, *Carbohydr. Polym.*, 1995, **27**, 191–195.
- 17 D.-L. Su, P.-J. Li, S. Y. Quek, Z.-Q. Huang, Y.-J. Yuan, G.-Y. Li and Y. Shan, *Food Chem.*, 2019, **286**, 1–7.
- 18 R. Xu and W.-J. Wu, *Food Res. Dev.*, 2012, **33**, 23–26.
- 19 P.-J. Li, J.-L. Xia, Z.-Y. Nie and Y. Shan, *Food Sci. Technol.*, 2016, **69**, 203–210.
- 20 P.-J. Li, J.-Y. Liang, D.-L. Su, Y. Huang, J.-J. Pan, M.-F. Peng and Y. Shan, *Bioprocess Biosyst. Eng.*, 2020, **43**, 2017–2026.
- 21 G. Wang, W. Jin, A. M. Qasim, A. Gao, X. Peng, W. Li, H. Feng and P. K. Chu, *Biomaterials*, 2017, **124**, 25–34.
- 22 P.-J. Li, J.-L. Xia, Z.-Y. Nie and Y. Shan, *Bioprocess Biosyst. Eng.*, 2016, **39**, 485–492.
- 23 H. Shi, *Experimental Guidance on Plant Stress Physiology*, Science Press, 2016.
- 24 S. A. El-Nawawi and Y. A. Heikal, *Carbohydr. Polym.*, 1995, **27**, 191–195.
- 25 P.-J. Li, J.-J. Pan, L.-J. Tao, X. Li, D.-L. Su, Y. Shan and H.-Y. Li, *Molecules*, 2021, **26**, 4479.
- 26 J. Yang, Y. Chen, L. Zhao, Z. Feng, K. Peng, A. Wei, Y. Wang, Z. Tong and B. Cheng, *Composites, Part B*, 2020, **197**, 108139.
- 27 K. Zheng, M. I. Setyawati, D. T. Leong and J. Xie, *Coord. Chem. Rev.*, 2018, **357**, 1–17.
- 28 N. K. Sharma, J. Vishwakarma, S. Rai, T. S. Alomar, N. AlMasoud and A. Bhattarai, *ACS Omega*, 2022, **7**, 27004–27020.
- 29 S. Vijayaram, H. Razafindralambo, Z.-y. Sun, S. Vasantharaj, H. Ghafarifarsani, S. H. Hoseinifar and M. Raeeszadeh, *Biol. Trace Elem. Res.*, 2024, **202**, 360–386.
- 30 D. Wang, W. Geng, Q. Li, G. Li, D. Zhang and H. Zhang, *Arabian J. Chem.*, 2022, **15**, 103500.
- 31 M. K. A. Al-Muhanna, K. S. Hileuskaya, V. I. Kulikouskaya, A. N. Kraskouski and V. E. Agabekov, *Colloid J.*, 2015, **77**, 677–684.
- 32 N. Yu, X. Wang, F. Ning, C. Jiang, Y. Li, H. Peng and H. Xiong, *Carbohydr. Polym.*, 2019, **217**, 58–68.
- 33 S. A. Ibraheem, E. A. Audu, A. J. Atabat, B. F. Tanimu, J. Y. Yahaya and J. T. Barminas, *Inorg. Chem. Commun.*, 2023, **158**, 111500.
- 34 G. Wang, X. Yang, X. Chen, J. Huang, R. He, R. Zhang and Y. Zhang, *Int. J. Biol. Macromol.*, 2024, **276**, 133798.
- 35 E. Z. Gomaa, *J. Gen. Appl. Microbiol.*, 2017, **63**, 36–43.
- 36 Y. G. Yuan, Q. L. Peng and S. Gurunathan, *Int. J. Mol. Sci.*, 2017, **18**, 569.
- 37 A. J. Kora and R. B. Sashidhar, *Arabian J. Chem.*, 2018, **11**, 313–323.
- 38 A. Rahal, A. Kumar, V. Singh, B. Yadav, R. Tiwari, S. Chakraborty and K. Dhama, *BioMed Res. Int.*, 2014, **2014**, 761264.

